ADVANCED MATERIALS

Table 1. n-Channel FET characteristics of BBL.

Thin film processing	Mobility (μ_e) [cm^2/Vs]	I_{on}/I_{off}	Threshold voltage (V_t)	Comment
MSA [a] (0.08 wt.-%)	$1.4–5.0 \times 10^{-4}$	30–150	–5	This Work
MSA/FA [b] (5:1, v/v) (0.07 wt.-%)	2.4×10^{-5}	8–30	–20	This Work
$FeCl_3$/NM [c] (0.1 wt.-%)	9×10^{-6}	<10	–5	This Work
$AlCl_3$/NM (n/a)	4×10^{-6}	2–50	n/a	Ref. [7]
$GaCl_3$/NM (n/a)	1×10^{-6}	2–50	n/a	Ref. [7]

[a] Methanesulfonic acid (MSA). [b] Formic acid (FA). [c] Nitromethane (NM).

ratios of up to 150 under ambient air conditions. This represents the highest field-effect mobility of electrons observed to date in a conjugated polymer. The observation of about 2 orders of magnitude variation in intrinsic mobility of electrons in BBL thin films due to changes in the solution processing methods (Table 1) suggests that future advances in the purification and control of the morphology of thin films will result in achievement of higher electron mobilities in this and related n-type conjugated polymers.

Experimental

BBL was synthesized as previously reported [15a]. The experimental details of BBL thin-film processing from Lewis acid/nitromethane and MSA solutions have been reported [11–15]. BBL thin films were spin cast onto gold patterned, oxide coated, silicon substrates. The 90 nm thick gold electrodes were sputtered onto a 10 nm thick Ti/W adhesive layer. The spin coated BBL thin film was partly removed from the gold electrodes to make electrical contacts to each FET device. Electrical characteristics of all devices were measured in ambient air at room temperature on a Hewlett-Packard (HP) 4155A semiconductor parameter analyzer.

BBL thin films spin coated from a 0.08 wt.-% solution in MSA were immersed in 10 % triethylamine solution in ethanol for at least 12 h, washed in water, and dried in a vacuum oven at 60 °C for 12–72 h. BBL thin films spin cast from 0.07 wt.-% solution in MSA/formic acid (5:1, v/v) were similarly treated. However, additional drying in vacuum at a higher temperature (200 °C) for 25 min was necessary to achieve FETs with drain current saturation (Fig. 4). BBL thin films spin coated from a 0.1 wt.-% solution in ferric chloride ($FeCl_3$)/nitromethane were immersed in methanol for 6 h and then water for 12 h to remove the ferric chloride. The resulting films were dried in vacuum at 60 °C for 6–72 h. $FeCl_3$ was used rather than $AlCl_3$ or $GaCl_3$ in order to do all the solution processing in ambient air.

Received: October 1, 2001
Final version: December 17, 2001

[1] Recent reviews: a) H. E. Katz, Z. Bao, *J. Phys. Chem. B* **2000**, *104*, 671. b) H. E. Katz, Z. Bao, S. L. Gilat, *Acc. Chem. Res.* **2001**, *34*, 359. c) C. D. Dimitrakopoulos, D. J. Mascaro, *IBM J. Res. Dev.* **2001**, *45*, 11. d) G. Horowitz, *Adv. Mater.* **1998**, *10*, 365.
[2] F. Garnier, G. Horowitz, D. Fichou, A. Yassar, *Synth. Met.* **1996**, *81*, 163.
[3] D. J. Gundlach, Y.-Y. Lin, T. N. Jackson, D. G. Schlom, *Appl. Phys. Lett.* **1997**, *71*, 3853.
[4] J. H. Schön, C. Kloc, B. Batlogg, *Science* **2000**, *288*, 2338.
[5] a) Z. Bao, A. Dodabalapur, A. J. Lovinger, *Appl. Phys. Lett.* **1996**, *69*, 4108. b) H. Sirringhaus, P. J. Brown, R. H. Friend, M. M. Nielsen, K. Bechgaard, B. M. W. Langeveld-Voss, A. J. H. Spiering, R. A. J. Janssen, E. W. Meijer, P. Herwig, D. M. de Leeuw, *Nature* **1999**, *401*, 685.
[6] C. J. Drury, C. M. J. Mutsaers, C. M. Hart, M. Matters, D. M. de Leeuw, *Appl. Phys. Lett.* **1998**, *73*, 108.
[7] X. L. Chen, Z. Bao, J. H. Schön, A. J. Lovinger, Y. Y. Lin, B. Crone, A. Dodabalapur, B. Batlogg, *Appl. Phys. Lett.* **2001**, *78*, 228.
[8] a) K. Wilbourn, R. W. Murray, *J. Phys. Chem.* **1988**, *92*, 3642. b) S. A. Jenekhe, *Polym. Mater. Sci. Eng.* **1989**, *60*, 419. c) X. L. Chen, S. A. Jenekhe, *Macromolecules* **1997**, *30*, 1728.
[9] a) T. Zheng, F. Badrum, I. M. Brown, D. J. Leopold, T. C. Sandreczki, *Synth. Met.* **1999**, *107*, 39. b) T. Yohannes, H. Neugebauer, S. Luzzati, M. Catellani, S. A. Jenekhe, N. S. Sariciftci, *J. Phys. Chem. B* **2000**, *104*, 9430.
[10] a) S. A. Jenekhe, J. A. Osaheni, *Science* **1994**, *265*, 765. b) J. A. Osaheni, S. A. Jenekhe, J. Perlstein, *J. Phys. Chem.* **1994**, *98*, 12 727. c) H. Antoniadis, M. A. Abkowitz, J. A. Osaheni, S. A. Jenekhe, M. Stolka, *Synth. Met.* **1993**, *60*, 149.
[11] a) S. A. Jenekhe, S. Yi, *Adv. Mater.* **2000**, *12*, 1274. b) S. A. Jenekhe, S. Yi, *Appl. Phys. Lett.* **2000**, *77*, 2635.
[12] a) S. A. Jenekhe, P. O. Johnson, *Macromolecules* **1990**, *23*, 4419. b) M. F. Roberts, S. A. Jenekhe, *Polymer* **1994**, *35*, 4313. c) S. A. Jenekhe, P. O. Johnson, A. K. Agrawal, *Macromolecules* **1989**, *22*, 3216.
[13] a) S. A. Jenekhe, S. J. Tibbetts, *J. Polym. Sci., Part B: Polym. Phys.* **1988**, *26*, 201. b) V. C. Long, S. Washburn, X. L. Chen, S. A. Jenekhe, *J. Appl. Phys.* **1996**, *80*, 4202. c) H. Antoniadis, M. A. Abkowitz, J. A. Osaheni, S. A. Jenekhe, M. Stolka, *Chem. Mater.* **1994**, *6*, 63.
[14] a) H. H. Song, A. V. Fratini, M. Chabinyc, G. E. Price, A. K. Agrawal, C.-S. Wang, J. Burkette, D. S. Dudis, F. E. Arnold, *Synth. Met.* **1995**, *69*, 533. b) H. H. Song, D. Y. Kim, *Bull. Korean Chem. Soc.* **1998**, *19*, 516.
[15] a) F. E. Arnold, R. L. Van Deusen, *Macromolecules* **1969**, *2*, 497. b) F. E. Arnold, R. L. Van Deusen, *J. Appl. Polym. Sci.* **1971**, *15*, 2035.

The Effect of Keto Defect Sites on the Emission Properties of Polyfluorene-Type Materials**

By *Emil J. W. List*,* *Roland Guentner*, *Patricia Scanducci de Freitas*, and *Ullrich Scherf*

Over the last years polyfluorenes (PFs)[1] have emerged as a promising class of conjugated polymers, which can be utilized as the blue light-emitting active layers in polymer light-emitting diodes (PLEDs),[2–4] as the host material for internal color conversion techniques,[5,6] or for PLEDs with polarized light emission,[7] exploiting the liquid crystalline nature of most of the PFs.

Yet, despite the ongoing improvements in terms of stability and color purity of PLEDs fabricated from PF type materials, most of these PLEDs suffer from a degradation of the device under operation documented in the formation of a low-energy emission band at 2.2–2.3 eV, which turns the desired blue emission color into an undesired blue–green emission. This band, which can also be found in photoluminescence (PL) emission upon photooxidation of the polymer, has been attributed to aggregation and/or excimer formation in the material.[8]

As presented in this paper, we have now identified this strong low-energy emission band at 2.2–2.3 eV using ultraviolet-visible (UV-vis) PL emission and infrared (IR) spectroscopy as the emission from exciton- and/or charge-trapping keto defect sites. We show that such keto defects, leading to the un-

[*] Dr. E. J. W. List
Institut für Festkörperphysik, Technische Universität Graz
Petersgasse 16, A-8010 Graz (Austria)
E-mail: e.list@tugraz.at
R. Guentner, Dr. P. Scanducci de Freitas, Prof. U. Scherf
Institut für Physikalische Chemie, Universität Potsdam
D-14476 Golm (Germany)

[**] This work was supported by SFB Elektroaktive Stoffe. The authors gratefully acknowledge the contribution of S. Mayer and A. Pogantsch for performing measurements and F. P. Wenzl and E. Zojer for fruitful discussions.

  0935-9648/02/0503-0374 $ 17.50+.50/0

wanted low-energy emission band in PFs, can be formed already during synthesis of a 9-monoalkylated PF (PF-a), or as a result of photo- (or electro-)oxidative degradation process of a 9,9-dialkylated PF (PF-b).

The presented data demonstrate that the keto defects act as low-energy trapping sites for singlet excitons, being populated by an excitation energy transfer from the PF main chain. Moreover, we find a much stronger contribution from the defect-related emission in electroluminescence (EL) than in PL, which is attributed to charge carrier trapping at the keto site in addition to trapping of singlet excitons at the keto defect sites. Our results indicate the key role of such keto defects for the emission properties of PF-type materials and PF-based light-emitting devices.

The 9-monoalkylated PF-a and the 9,9-dialkylated PF-b were synthesized from the corresponding 2,7-dibromofluorene monomers in a reductive aryl–aryl coupling according to Yamamoto. Since the coupling of the dialkyl monomer leads to the expected high molecular weight PF with a unimodal molecular weight distribution, the condensation of the monoalkylated monomer leads to lower molecular weight products with a broader, bimodal molecular weight distribution. This indicates the occurrence of side reactions during the reductive coupling of the monoalkylated dibromofluorene monomer.

As depicted in Figure 1a, PF-a in dilute solution exhibits a broad absorption peak at 3.2 eV and a PL emission spectrum showing maxima at 2.95 eV and 2.8 eV as well as an unexpected low-energy band peaking at 2.35 eV. In the solid state the absorption of PF-a becomes much broader and an additional contribution centered at ca. 2.8 eV occurs. In contrast to the emission spectrum of PF-a in toluene solution, the solid-state PL spectrum is dominated by the low-energy emission peak at 2.33 eV.

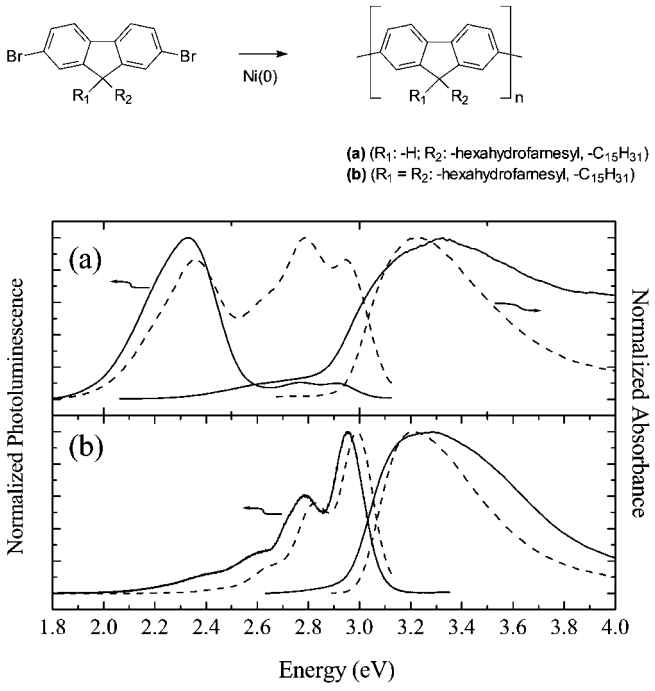

Fig. 1. Top: Synthesis of 9-mono- and 9,9-dialkylated PFs (PF-a and PF-b, respectively). Bottom: a) absorbance and PL emission of PF-a in toluene solution (dashed line) and in the solid state (solid line), b) absorbance and PL emission of PF-b in toluene solution (dashed line) and in the solid state (solid line).

Contrary to PF-a, the dialkylated PF (PF-b) exhibits very similar absorption and emission properties both in toluene solution and in the solid state, as depicted in Figure 1b. The absorption spectra of both solution and film are dominated by one broad absorption feature peaking at 3.3 eV with the solid-state spectrum being slightly broadened. The PL emission spectrum of the PF-b solution shows the π^*–π transition of the conjugated PF backbone at 3.0 eV[9] with well-resolved vibronic replica at 2.82 eV and 2.63 eV. All features of the film display a slight bathochromic shift of ca. 50 meV.

Comparing the energetic position of the π^*–π transition at 3.0 eV and its vibronic replica in the PL spectrum of PF-b with the emission peaks in PF-a found at 2.95 eV and 2.8 eV these transitions are assigned to the emission from the delocalized π-electron system of the PF main chain. On the contrary the low-energy emission band at 2.3 eV, which is only found in PF-a, has a different origin that is not related to the emission from the PF backbone. From a comparison with literature results we now assign this emission band to the presence of keto defect sites, namely fluorenone building blocks, which have been found to emit exactly at this energetic position.[10] As explained in detail below, the keto defect sites present in monoalkylated PF-a are formed already during the synthesis of the polymer. In dialkylated PF-b such keto defect sites are not detectable after polymer synthesis but can be created during an oxidative photo-degradation process (see below). The assignment of the low-energy emission band to the presence of yellow/orange emitting fluorenone defect sites is in agreement with the observation of an additional IR band at ca. 1721 cm^{-1} in pristine PF-a samples as shown in Figure 2a. This signal is not detectable in pristine PF-b as depicted in the same figure. This band has been identified as the carbonyl stretching mode (>C=O) of the fluorenone building block.[11] Furthermore, the weak low-energy tail of the PF-a absorption in toluene solution at ca. 3.0 eV, and more pronounced and bathochromically shifted in the solid state at ca. 2.8 eV, is identified as the absorbance of the fluorenone chromophores (π–π^* transition).[10] This low-energy absorption tail/shoulder is absent in pristine PF-b both in diluted solution and the solid state.

The energetic position of the low-energy emission band at ca. 2.3 eV in PF-a is very similar to the low-energy emission band of the fluorenone building block in statistical dialkylfluorene/fluorenone copolymers,[12] as well as in photooxidized (photodegradated) fluorene-endcapped poly(9,9-dihexylfluorene) as demonstrated by other investigators.[13] Hereby, the terminating unsubstituted fluorene moieties are oxidized to fluorenone units. These findings strongly support the presented assignment of our experimental results. In this light, the often favored interpretation of the low-energy emission bands in PF (and also in ladder-type poly(*para*-phenylene)s LPPP, in which such low-energy emission bands also occur at

  0935-9648/02/0503-0375 $ 17.50+.50/0

ADVANCED MATERIALS

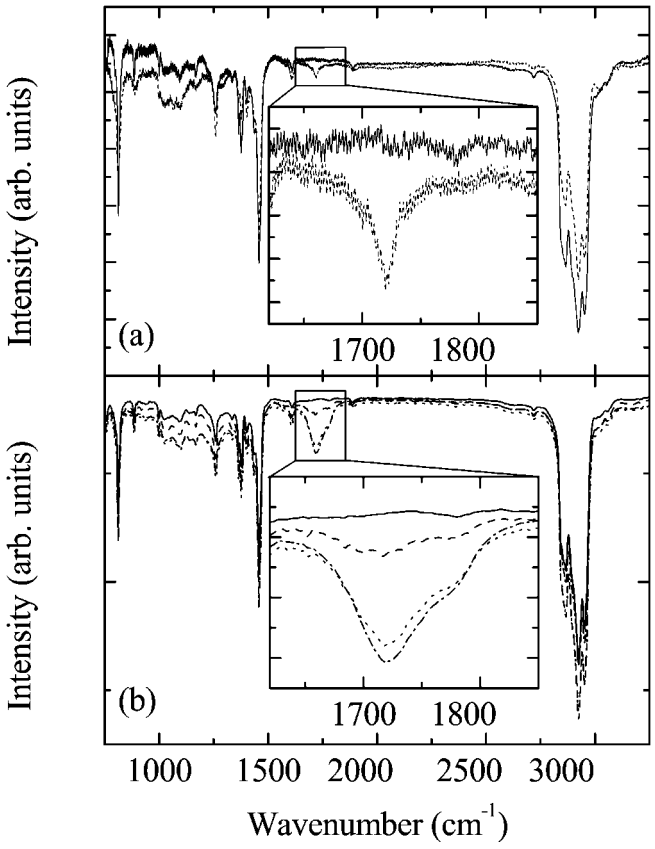

Fig. 2. IR transmission spectra of polymer films on Si. a) PF-a film (dashed line) and PF-b film on Si (solid line), b) pristine PF-b film (solid line), after photooxidation with a 1000 W xenon lamp under air for 2 min (dashed line), 4 min (dotted line), and 6 min illumination (dash-dotted line). The insets in either plot show the >C=O stretching mode at 1721 cm^{-1} magnified for better visibility.

a similar spectral position of ca. 2.2 eV!) with an ongoing aggregate or excimer formation[8] is at the very least questionable.

In contrast, we propose that the keto defects act as "guest" emitters, which efficiently trap singlet excitons created on the conjugated PF backbone by a dipole–dipole induced direct excitation energy transfer of the Förster-type[14] or an excitation energy migration (EEM) assisted Förster-type transfer process.[15,16] This process becomes the dominating channel of excited state depopulation in the solid state. Due to the reduced interchain Förster-type or fully inhibited EEM assisted energy transfer to the keto defect sites for dilute solutions, the contribution of the low-energy band at 2.3 eV in dilute solutions of PF-a is only moderate. Moreover, as discussed in detail elsewhere, we have performed correlated quantum-chemical simulations to gain a deeper insight into the nature of the electronic states involved in the absorption and emission processes in these materials.[17] We have studied the excited as well as ground state conformations coupling the intermediate neglect of differential overlap (INDO) Hamiltonian to a configuration interaction (CI) approach. For the keto defect sites containing PF, these calculations show a localization of the emissive excited state on the fluorenone unit prior to recombination, while the emissive excited state is delocalized over several fluorene segments in pristine PF. These findings indicate that the exciton localization effect at the fluorenone unit enhances the emission of keto defect sites in addition to excitation energy transfer processes in such materials.

The herein presented spectroscopic results prove the presence of keto trapping sites in pristine 9-monoalkylated PF-a already after polymer synthesis. As depicted in Figure 3 the generation of the fluorenone defect sites can be explained by

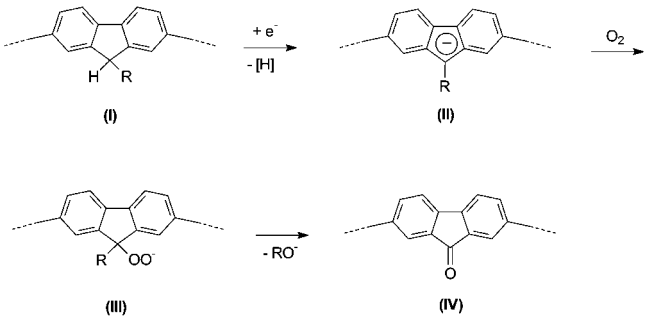

Fig. 3. Proposed mechanism for the generation of keto defect sites (explanation: see text).

the following chemical mechanism: The highly active Ni^0 species used in the reductive coupling of the dibromo monomers reduce a certain amount of the 9-monoalkylated fluorene building blocks (I) to (aromatic) fluorenyl anions (II) under formation of hydrogen. These anions can form hydroperoxide anions (III) with atmospheric oxygen during the work-up of the reaction mixture. The hydroperoxide anions then undergo a final rearrangement to fluorenone moieties (IV).

The formation of a certain amount of keto defect sites during the synthesis of 9-monoalkylated polyfluorene PF-a leads to the previously outlined spectroscopic behavior. However, such keto defect sites can not only be formed as side reaction during polymer synthesis, as shown for PF-a, but can be also formed as a result of a photo- or electrooxidative degradation of 9,9-dialkylated polyfluorene PF-b. In order to demonstrate the degradation-induced creation of keto-defects, PF-b samples were studied in photooxidation (depicted in Fig. 4) as well as in electrooxidation experiments (depicted in Fig. 5).

Figure 4 shows the PL spectrum of a pristine PF-b film and of the subsequently degraded sample. A photooxidation of the sample for 6 min results in a dramatic decrease of the integral PL yield to approximately 10 % of the initial value. Simultaneously, the low-energy emission band at 2.3 eV emerges, which increases in intensity relative to the PF emission for increasing photooxidation of PF-b. Furthermore, in the simultaneously measured IR spectra (depicted in Fig. 2b) one finds the appearance of the fluorenone site (>C=O stretching mode) at 1721 cm^{-1}, which increases for increasing degradation of the sample. These findings clearly show that emissive fluorenone keto-defects are introduced upon degradation and yield the lower energy emission band at 2.3 eV.

Figure 5 depicts the EL spectrum of an indium tin oxide (ITO)/PF-a/Al device (PLED) (solid line), an ITO/PF-b/Al device (dashed line), and an ITO/PF-b/Al device after 30 min

  0935-9648/02/0503-0376 $ 17.50+.50/0

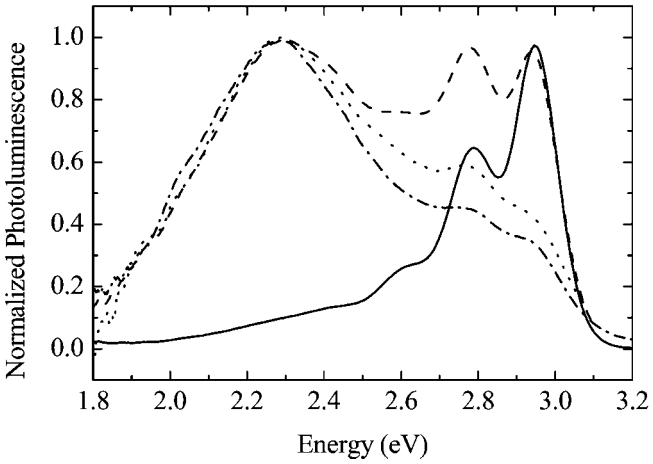

Fig. 4. PL emission spectrum of a pristine PF-b film (solid line), and after photooxidation with a 1000 W xenon lamp under air for 2 min (dashed line), 4 min (dotted line), and 6 min illumination (dash-dotted line).

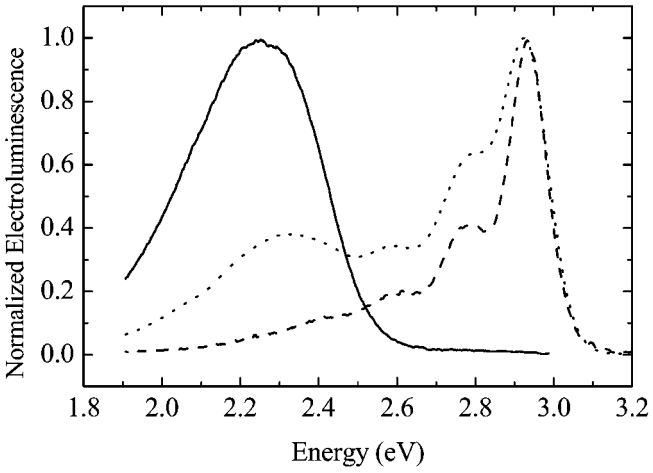

Fig. 5. EL spectrum of an ITO/PF-a/Al device (solid line), an ITO/PF-b/Al device (dashed line), and this ITO/PF-b/Al device after 30 min continuous operation under air (dotted line).

of continuous operation at 14 V and a current density of 1 mA/cm^2 under air. The EL spectrum of the PF-a device is fully dominated by the low-energetic emission band at ca. 2.25 eV leading to a yellow–orange emission, similar to the emission found for a PLED with poly(9-fluorenone) as emissive layer.[18] However, the emissive contribution of keto defect sites is more pronounced in EL devices when compared to our PL experiments. The reason for this behavior is the presence of two parallel processes that give a low-energy EL contribution due to the presence of fluorenone defect sites: a) energy transfer of singlet excitons from the PF main chain to keto defect sites and b) trapping of charges at the fluorenone defect sites and their subsequent emissive recombination. The second process cannot proceed in PL experiments and increases the contribution of the defect-site-related low-energy EL band. Therefore, in contrast to the PL process, in EL devices a much lower concentration of fluorenone defects results in a dominating low-energy emission band.[19,20]

For the PF-b-based EL devices (PLEDs), a stable and efficient blue emission occurs at turn-on voltages of ca. 8 V.[21] However, the color changes into a blue–greenish emission after more than 30 min of continuous operation in air. The EL spectrum then exhibits an additional low-energy emission band at ca. 2.3 eV, which we also assign to the formation of fluorenone defect sites. This finding demonstrates that the formation of fluorenone defect sites also occurs during operation of PLEDs based on 9,9-dialkylated PF-b, especially under atmospheric conditions.

Our novel results strongly indicate the key role of keto defect sites as source of low-energy emission bands, most pronouncedly for PFs with methylene bridged hydrogen substituents. The findings illustrate the superiority of a difunctionalization at the methylene group in all –CR_2– bridged polyphenylene and polyarylene derivatives (e.g., PF, but also in LPPPs). As demonstrated previously, also the shielding of the PF backbone with dendritic side chains leads to an increased chemical stability and reduced interchain energy transfer.[22] However, the photo- or electrooxidative degradation processes, which lead to similar low-energy emission bands in disubstituted, "hydrogen-free" PF and LPPP derivatives (e.g., poly(9,9-dioctylfluorene) (PFO), MeLPPP[23,24]) have to be studied further, especially in order to improve the long-term and color stability of polyarylene-based blue PLEDs.

Experimental

Polymer Synthesis: All reactions were carried out in an argon atmosphere. The solvents were used as commercial p.a. quality. ^{1}H and ^{13}C nuclear magnetic resonance (NMR) data were obtained on a Bruker DPX 400 spectrometer. Gel permeation chromatographic analysis (GPC) utilized polystyrene (PS)-columns (three columns, 5 μm gel, pore widths 10^2, 10^3, and 10^5 Å) connected with UV-vis/refractive index (RI) detection. All GPC analyses were performed on solutions of the polymers in chloroform at 30 °C (concentration of the polymer = 1.5 g/L). The calibration was based on PS standards with narrow molecular weight distribution. The monomers 9,9-bis(3,7,11-trimethyldodecyl)-2,7-dibromofluorene and 9-(3,7,11-trimethyldodecyl)-2,7-dibromofluorene were synthesized in close analogy to the method described previously [25]. (3,7,11-Trimethyldodecyl = hexahydrofarnesyl).

Poly(2,7-(9,9-bis(3,7,11-trimethyldodecyl)fluorene): A solution of 2.0 mmol 9,9-bis(3,7,11-trimethyldodecyl)-2,7-dibromofluorene in 10 mL of dry toluene was added at 80 °C to a solution of 4.6 mmol Ni(COD)$_2$ (COD = cyclooctadiene), 4,6 mmol 2,2′-bipyridyl, and 2.4 mmol COD in 4 mL of dry dimethylformamide/10 mL of dry toluene. The mixture was stirred for 5 days at 80 °C and quenched with 4 M hydrochloric acid in dioxane. The polymer was precipitated in a mixture of methanol/acetone/2 M hydrochloric acid and extracted with ethyl acetate for 5 days. Finally, the polymer was redissolved in chloroform, the solution concentrated, the polymer reprecipitated, and dried for 48 h in vacuum at room temperature. Yield: 60 %.

^{13}C NMR (100 MHz, $C_2D_2Cl_4$, 353 K): δ [ppm] 151.5, 140.9, 140.3, 126.4, 122.0, 120.1, 55.4, 39.7, 37.7, 37.6, 37.3, 33.3, 33.2, 33.0, 31.3, 29.9, 28.1, 24.9, 24.7, 22.9, 22.8, 19.9.

^{1}H NMR (400 MHz, $C_2D_2Cl_4$, 353 K): δ [ppm] 8.00–7.20 (6H), 2.35–1.90 (10H), 1.50–0.45 (52H). M_n = 80 000. M_w = 197 400. M_w/M_n = 2.5. M_p = 159 700.

Poly(2,7-(9-(3,7,11-trimethyldodecyl)fluorene)): Please see the above procedure for poly(2,7-(9,9-bis(3,7,11-trimethyldodecyl)fluorene)). Yield: 29 %.

^{13}C NMR (100 MHz, $C_2D_2Cl_4$, 353 K): δ [ppm] 149.0, 140.6, 140.3, 126.5, 123.4, 120.4, 39.7, 37.7, 37.6, 37.3, 33.3, 33.2, 33.0, 31.3, 29.9, 28.1, 24.9, 24.7, 22.9, 22.8, 19.9.

^{1}H NMR (400 MHz, $C_2D_2Cl_4$, 353 K): δ [ppm] 8.00–7.20 (6H), 4.10 (1H), 2.35–1.90 (5H), 1.50–0.45 (26H). M_n = 23 920. M_w = 275 200. M_w/M_n = 11.5. M_{p1} = 18 000. M_{p2} = 61 600 (bimodal molecular weight distribution).

Materials Characterization and Devices: UV-vis transmission spectra were measured using a Perkin-Elmer λ9 spectrophotometer. PL emission and excita-

  0935-9648/02/0503-0377 $ 17.50+.50/0

ADVANCED MATERIALS

tion spectra were recorded using a Shimadzu RF5301 spectrofluorometer. EL spectra were recorded using an ORIEL spectrometer with an attached charge coupled device (CCD) camera. A 1000 W halogen lamp provided the source for the photooxidation measurement. The ITO covered glass substrates for the PLEDs were thoroughly cleaned in a variety of organic solvents. The Al metal electrodes were thermally deposited in a Baltzers MED010 vacuum coating unit at base pressures of below 5×10^{-6} mbar.

Received: August 9, 2001
Final version: December 6, 2001

[1] M. T. Bernius, M. Inbasekaran, J. O'Brien, W. Wu, *Adv. Mater.* **2000**, *12*, 1737.
[2] M. Gross, D. C. Müller, H.-G. Nothofer, U. Scherf, D. Neher, C. Bräuchle, K. Meerholz, *Nature* **2000**, *405*, 661.
[3] A. W. Grice, D. D. C. Bradley, M. T. Bernius, M. Inbasekaran, W. W. Wu, E. P. Woo, *Appl. Phys. Lett.* **1998**, *73*, 629.
[4] R. H. Friend, R. W. Gymer, A. B. Holmes, J. H. Burroughes, R. N. Marks, C. Taliani, D. D. C. Bradley, D. A. Dos-Santos, J. L. Brédas, M. Lögdlund, W. R. Salaneck, *Nature* **1999**, *397*, 121.
[5] T. Virgili, D. G. Lidzey, D. D. C. Bradley, *Adv. Mater.* **2000**, *12*, 58.
[6] P. A. Lane, L. C. Palilis, D. F. O'Brien, C. Giebeler, A. J. Cadby, D. G. Lidzey, A. L. Campbell, W. Blau, D. D. C. Bradley, *Phys. Rev. B* **2001**, *63*, 235 206.
[7] M. Grell, W. Knoll, D. Lupo, A. Meisel, T. Miteva, D. Neher, H.-G. Nothofer, U. Scherf, A. Yasuda, *Adv. Mater.* **1999**, *11*, 671.
[8] a) U. Lemmer, S. Heun, R. F. Mahrt, U. Scherf, M. Hopmeier, U. Siegner, E. O. Göbel, K. Müllen, H. Bässler, *Chem. Phys. Lett.* **1995**, *240*, 373. b) E. Conwell, *Trends Polym. Sci.* **1997**, *5*, 218. c) M. Grell, D. D. C. Bradley, G. Ungar, J. Hill, K. S. Whitehead, *Macromolecules* **1999**, *32*, 5810. d) V. Cimrová, U. Scherf, D. Neher, *Appl. Phys. Lett.* **1996**, *69*, 608.
[9] A. J. Cadby, P. A. Lane, H. Mellor, S. J. Martin, M. Grell, C. Giebeler, D. D. C. Bradley, *Phys. Rev. B* **2000**, *62*, 15 604.
[10] M. Ilharco, R. Garcia-Ana, J. Lopes-da-Silva, M. Joao-Lemos, L. F. Vieira-Ferreira, *Langmuir* **1997**, *13*, 3787.
[11] R. M. Silverstein, G. C. Bassler, T. C. Morrill, *Spectroscopic Identification of Organic Compounds*, 4th ed., Wiley, New York **1981**.
[12] H.-G. Nothofer, *Ph.D. Thesis*, University of Potsdam **2001**.
[13] a) V. N. Bliznyuk, S. Carter, J. C. Scott, G. Klärner, R. D. Miller, D. C. Miller, *Macromolecules* **1999**, *32*, 361. b) J. I. Lee, G. Klärner, R. D. Miller, *Chem. Mater.* **1999**, *11*, 1083.
[14] T. Förster, *Ann. Phys.* **1948**, *2*, 55.
[15] E. J. W. List, C. Creely, G. Leising, N. Schulte, A. D. Schlüter, U. Scherf, K. Müllen, W. Graupner, *Chem. Phys. Lett.* **2000**, *325*, 132.
[16] A. R. Buckley, M. D. Rahn, J. H. Hill, J. Cabanillas-Gonzalez, A. M. Fox, D. D. C. Bradley, *Chem. Phys. Lett.* **2001**, *339*, 331.
[17] E. Zojer, A. Pogantsch, E. J. W. List, R. Guentner, P. S. de Freitas, R. Guentner, P. Scanducci de Freitas, U. Scherf, J. L. Brédas, unpublished results.
[18] F. Uckert, Y.-H. Tak, K. Müllen, H. Bässler, *Adv. Mater.* **2000**, *12*, 905.
[19] E. J. W. List, G. Leising, N. Schulte, A. D. Schlüter, U. Scherf, W. Graupner, *Jpn. J. Appl. Phys.* **2000**, *39*, L760.
[20] S. Tasch, E. J. W. List, C. Hochfilzer, G. Leising, P. Schlichting, U. Rohr, Y. Geerts, U. Scherf, K. Müllen, *Phys. Rev. B* **1997**, *56*, 4479.
[21] The elevated turn-on voltages of the presented PLEDs are due to the use of a high work function metal (Al) as top metal electrode, which has been chosen to avoid possible influences of a metal–polymer interface reaction.
[22] S. Setyesh, A. C. Grimsdale, T. Weil, V. Enkelmann, K. Müllen, F. Meghdadi, E. J. W. List, G. Leising, *J. Am. Chem. Soc.* **2001**, *123*, 946.
[23] W. Graupner, J. Partee, J. Shinar, G. Leising, U. Scherf, *Phys. Rev. Lett.* **1996**, *77*, 2033.
[24] J. Teetsov, M. A. Fox, *J. Mater. Chem.* **1999**, *19*, 2117.
[25] E. P. Woo, M. Inbasekaran, W. Shiang, G. R. Roof, *Int. Pat. Appl. WO 97/05 184*, **1997**.

The Core–Shell Approach to Formation of Ordered Nanoporous Materials**

By *Jeong Ho Chang*, *Li-Qiong Wang*, *Yongsoon Shin*, *Byeongmoon Jeong*, *Jerome C. Birnbaum*, and *Gregory J. Exarhos**

This work describes an innovative approach for the preparation of ordered nanoporous ceramic materials that involves a self-assembly process at the molecular level based upon monomethoxy poly(ethylene glycol)-*block*-poly(D,L-lactide) (MPEG-*b*-PDLLA) block copolymer templates. This approach is suitable for rapid self-assembly and structural reorganization at room temperature. Selected MPEG-*b*-PDLLA block copolymers have been synthesized with systematic variation of the chain lengths of the resident hydrophilic and hydrophobic blocks. The size and shape of the micelles that spontaneously form in solution are then controlled by the characteristics of the copolymer template. Formation of nanoporous silica at room temperature with short preparation time is demonstrated and silica-containing materials evolve with uniform pore shape and wall structure. The formation mechanism of these nanoporous structures obtained by controlling the micelle size has been confirmed using both liquid- and solid-state ^{13}C and ^{29}Si nuclear magnetic resonance (NMR) techniques. This work both proposes and verifies the formation mechanism of nanoporous structures in which the pore size and wall thickness are closely dependent on the size of hydrophobic cores and hydrophilic shells of the block copolymer templates.

Molecularly controlled synthesis of nanoporous materials is an area of burgeoning interest and is driven by their potential applications in next generation catalysts and photonic materials.[1–6] The general route for preparation of these molecularly ordered inorganic materials involves an organic-templating technique based upon the electrostatic and/or sterically controlled assembly of commercial amphiphilic organic surfactants such as cetyltrimethylammonium bromide (CTAB) or non-ionic polyethylene oxide surfactants.[7–9] Until now, many studies adopted these methods and demonstrated ordered materials with high surface area and uniform pore structures. The MCM-41 and Santa Barbara Acidic Materials (SBA) type materials are frequently studied among these porous materials because they exhibit well-ordered pore arrays that can be modified by varying the alkane chain length of the ionic sur-

[*] Dr. G. J. Exarhos, Dr. J. H. Chang, Dr. L.-Q. Wang, Dr. Y. Shin, Dr. B. Jeong, Dr. J. C. Birnbaum
Pacific Northwest National Laboratory
Battelle Boulevard, PO Box 999/MS K2-44
Richland, WA 99352 (USA)
E-mail: greg.exarhos@pnl.gov

[**] Pacific Northwest National Laboratory is operated for the U.S. Department of Energy by Battelle Memorial Institute under Contract DE-AC06-76RL0 1830. This work derives support from the Division of Materials Sciences and Engineering Division of Basic Energy Sciences within the Office of Science, U.S. Department of Energy.

  0935-9648/02/0503-0378 $ 17.50+.50/0